PROCEEDINGS OF ECOS 2023 - THE 36TH INTERNATIONAL CONFERENCE ON
EFFICIENCY, **C**OST, **O**PTIMIZATION, **S**IMULATION AND ENVIRONMENTAL IMPACT OF ENERGY SYSTEMS
25-30 JUNE 2023, LAS PALMAS DE GRAN CANARIA, SPAIN

Stability and Reserve Constraints in Optimal Dispatch Models for Poorly Interconnected Countries of the Global South

Marco Navia[a], Matija Pavičević[b], Sergio Balderrama[c] and Sylvain Quoilin[d]

[a] Université de Liège, Liege, Belgium, manavia@uliege.be
[b] UC Louvain la Neuve, Leuven, Belgium, matija.pavicevic@uclouvain.be
[c] Universidad Mayor de San Simon, Cochabamba, Bolivia, s.balderrama@umss.edu
[d] Université de Liège, Liege, Belgium, squoilin@uliege.be

Abstract:
The United Nations Framework Convention on Climate Change (UNFCCC) is strongly committed to accelerating the transition of the power sector towards a high penetration of Variable Renewable Energy (VRE) sources, with the goal of reducing global dependence on fossil fuels for power generation. However, this transition poses a significant challenge, as the increasing VRE share in power systems gradually decreases their rotational inertia. This reduction in rotational inertia negatively impacts the stability and safety of power systems, creating new operational challenges. To address this, transmission system operators (TSO) have defined strategies to compensate for unexpected imbalances between load and generation by contracting primary and secondary reserves. Nevertheless, a method that compensates for the inertial response excursion after a disturbance adapted to these tools has not yet been fully identified. This work proposes a deterministic estimation of inertia constraint in UC/OD models. The Rate of change of Frequency (RoCoF) is estimated from an Optimal Dispatch model by considering the worst-case contingency in the test case. Then the lower inertia limit required to operate the system with stability is estimated. The estimation of the inertia limit is done offline the optimization and added as a new constraint in the UC/OD model. Finally, different scenarios of VRE penetration are defined to evaluate the impact of this new constraint with a sensitivity analysis. Results show that the proposed method can be complementary applied to UC/OD models to reduce the risk of unintended load shedding, which might lead to cascading failures and blackouts.

Keywords:
VRE, Energy, Inverter-based generation, Inertia estimation, Low-Inertia power systems, Energy Systems Modeling, Power Systems Modeling, Power Systems Stability, Unit-Commitment, Optimal Dispatch, TSOs, ECOS Conference, Energy Transition, Sustainability.

1. Introduction and Problem description

The UNFCCC has consistently emphasized the urgency of reducing carbon emissions in the power sector as part of Sustainable Development Goal 7 (SDG7) [1]. According to the International Energy Agency's (IEA) World Energy Outlook [2], numerous regions worldwide, such as Central and South America, the European Union, the United States, and Asia, are making substantial progress in deploying variable renewable energy (VRE) in electricity generation. It is expected that the shares of VRE could increase from 28% in 2021 to approximately 50% by 2030 and 80% by 2050. This new context leads to a fundamental shift in the production and consumption of electricity.

At the operational stage, there are two main linked issues that are slowing down the pace of the energy transition because they fundamentally impact the security of power systems and supply reliability [3]. The first issue is the intermittent generation, which exposes the power systems to a more dynamic behavior due to unexpected imbalances between load and generation. These imbalances may be caused by factors such as tripping of generating units, inaccuracies in load forecast methods, or unexpected deviations by generating units from their dispatch schedules [4]. The second issue is the progressive replacement of traditional synchronous generators with inverter-based generation. This reduces the system's inertia, accelerating the Frequency Response (FR) excursion and declining mainly the Inertial Response time frame [5, 6].

FR is the power variation during the generation-load imbalance affected automatically by the power system itself due to frequency changes alone [7]. During the imbalance between generation and demand, FR elapses progressively within different time frames in the power system. Fig.1 shows typical frequency excursions after a generator outage. The FR excursion includes the inertial ($<$10 s), primary (10s–30s), and secondary responses (minutes). While operating reserve compensation schemes are currently activated to restore normal

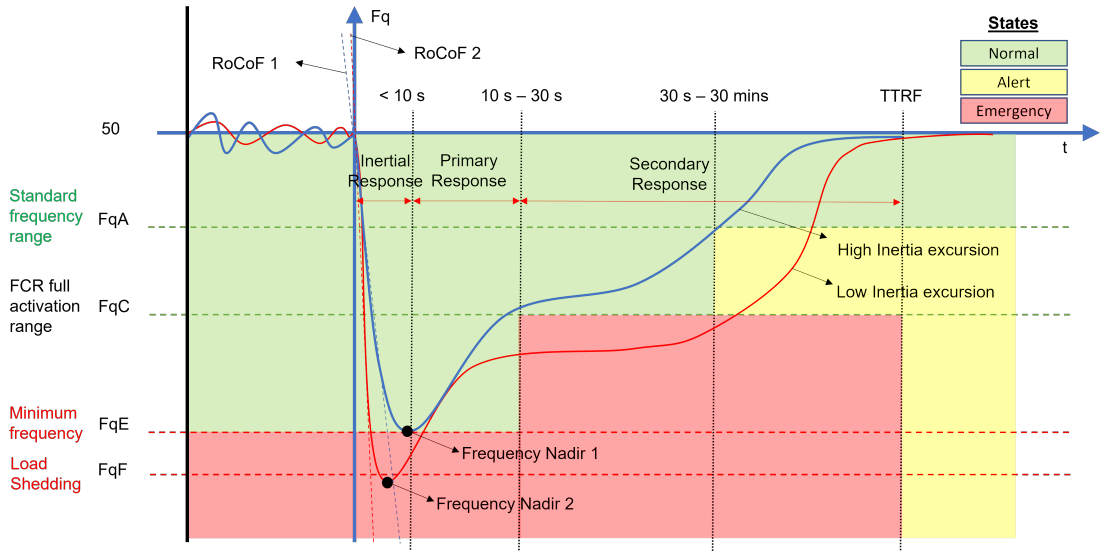

Figure 1: Generic Frequency responses excursions and different times frames in power systems. [8]

power system operation [9]. These corrective actions only address the primary and secondary response time frames. Moreover, they only occur after the inertial response if the frequency nadir(the lowest point the frequency reaches during an event) and the rate of change of frequency (RoCoF) do not reach blackout-inducing levels. Thus, it is crucial to investigate the inertial response frame.

To stop the frequency decline and avoid operating in an emergency state during the inertial response, the power system relies on the kinetic energy stored in synchronous generators (inertia). In systems with low inertia, such as those with a high penetration of renewable energy sources, the inertial response may be insufficient to stabilize the system, leading to frequency instability, unintended triggering of under-frequency protection, load-shedding, and potential blackouts (e.g., Australia [10], 2016; and the United Kingdom, 2019 [11]) [12, 13]. Consequently, there has been a surge of interest in devising strategies to enhance the inertia of power systems. Proposed solutions entail enhancing grid flexibility, through the use of energy storage systems [14], and deploying sophisticated forecasting techniques [15]. Other measures include promoting demand response [16], enforcing grid codes [17], and utilizing virtual inertia [18]. Although many solutions have been proposed to address stability issues, the Fast Frequency Reserve (FFR) presented in [19] address more specifically the inertial response frame. This new reserve consist in a system of Reserve Units that automatically activate to restore stability after a disturbance, and their power output adjusts based on frequency measurement during stability recovery. FFR is primarily being evaluated and implemented in advanced countries with high VRE penetration, where the issue is most pronounced. However, these solutions are even less widely adopted in developing countries with poor interconnections and may require context-specific adaptations.

Therefore, it is crucial to develop effective methods to enhance the inertial response frame and ensure system stability, specially for regions that are recently increasing their shares of VRE into their energy mix. In this regard, advanced studies have proposed different approaches to address this issue in the context of unit commitment and economic dispatch (UC/OD). For instance, [20] proposed a methodology that linearizes frequency response (FR) constraints into the ordinary UC formulation under high variable renewable energy (VRE) penetration, using deep neural networks (DNNs) to acquire FR predictions. Similarly, [21] presented a coordination between wind power and thermal units to achieve frequency-secured UC under significant wind power uncertainty. However, this work focuses on proposing a simplified offline method for estimating the inertia limit that meets the stability requirements of the system under a worst-case scenario. Additionally, the implementation of the estimated inertia limit as a new constraint for the global optimization of the UC/OD model is proposed.

2. Methodology

2.1. Workflow

In this paper, the inertia requirement of a power system under the safety limits of operation is estimated using a deterministic approach to avoid extensive computational time associated with reproducing stochastic behavior. The work is proposed in stages, as shown in Fig.2. Every stage of the methodology will be developed in the following sections.

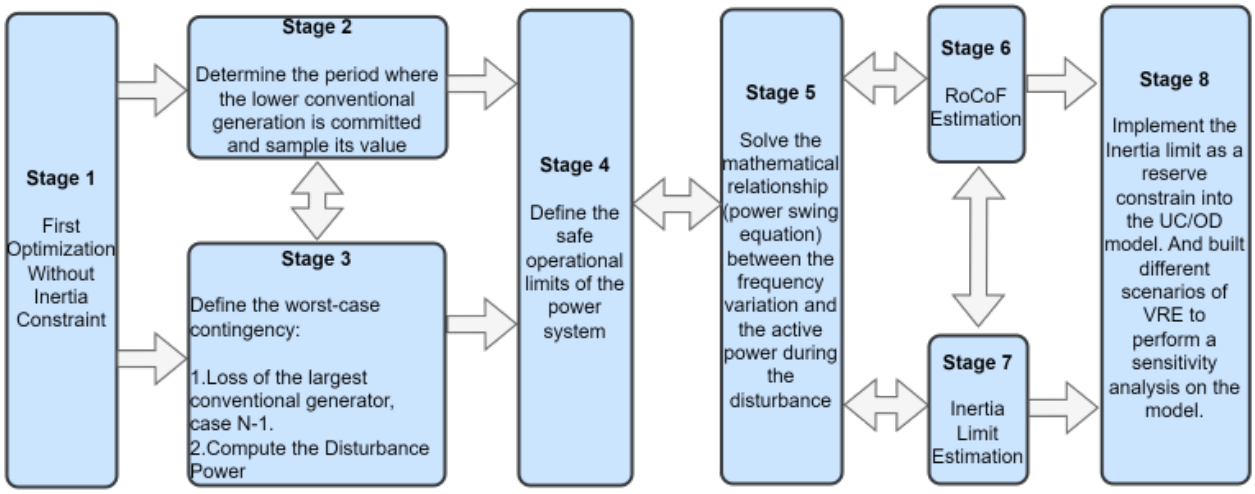

Figure 2: Workflow.

2.2. Definitions and Equations

2.2.1. Minimum Conventional Power Committed

The region of sampling is defined as the period with the minimum conventional power capacity committed and is determined using the baseline dispatch, with the following equations:

$$MinCommitted = Min\left(\sum_{cu} PowerCapacity_{cu,i} \cdot Committed_{cu,i}\right) \tag{1}$$

$$P_{PreDist} = MinCommitted \tag{2}$$

Where:

- i is the set for time-step in the current optimization horizon.
- cu is the set defined for all the conventional units.
- $PowerCapacity_{cu}$ is the power rating for each conventional generation unit.
- $Committed_{cu,i}$ is the binary commitment status (1 or 0) for each conventional generation unit at each time-step of simulation.
- $MinCommitted$ is the minimum conventional power capacity committed.
- $P_{PreDist}$ is pre-distortion power committed sampled from the baseline dispatch.

2.2.2. Worst-case Contingency

The worst-case Contingency is defined as the loss of the largest conventional unit. It is expressed in terms of power per unit of the power committed left after the disturbance. It is determined with the equations below:

$$P_{MaxGen} = Max\left(PowerCapacity_{cu}\right) \tag{3}$$

$$P_{Loss} = \frac{P_{MaxGen}}{P_{PreDist} - P_{MaxGen}} \tag{4}$$

Where:

- P_{MaxGen} is the power capacity of the largest generator.
- P_{Loss} is the power change after a disturbance, expressed in per unit of the system load base.

2.2.3. Safe Operational Limits: Post-Fault Frequency

The frequency nadir represents the lowest frequency reached during the transient period, while the recovery time refers to the time it takes for the frequency corrective actions (FCA) to activate. Transmission System Operators (TSOs) can establish multiple activation levels of FCA. This study considers only under-frequency events; regarding the post-fault frequency limits, the values defined in this study were taken from [22] with the following adaptations:

- *RoCoF* must be above -0.125Hz/s ($RoCoF_{Limit}$) at all times to avoid tripping *RoCoF*-sensitive protection relays.
- The frequency nadir must never be below 49.2Hz ($f_{NadirLimit}$) to prevent the activation of Under Frequency Load Shedding (i.e. $\Delta fmax$ = 0.8Hz).
- Frequency must recover from being above 49.5Hz within 60s after the outage, referred to as the frequency quasi-steady state requirement (i.e. $\Delta fssmax$ = 0.5Hz).

2.2.4. Solving the Power Swing Equation

The power swing equation expresses the electromechanical dynamics of a power system. Under the assumption that the generators stay synchronized after a disturbance (all generators of the system swing together), they will have a similar frequency trajectory with inter-mutual swings. To apply the swing equation to the whole power system, a representative average frequency signal (frequency of the center of inertia) of the system is defined as which is defined as f_{COI}, and the power swing equation can be expressed as follows:

$$2 \cdot H_{Sys} \cdot \frac{d\Delta f_{COI}}{dt} = \Delta P_m - \Delta P_e = \Delta P \tag{5}$$

Where:

- H_{Sys} is the average inertia constant of the power system, and its value is expressed in sec.
- $d\Delta f_{COI}/dt$ is the variation of the system frequency signal in time, and its value is expressed in pu/sec.
- ΔP_m is the total mechanical power deviation, and its value is expressed in pu.
- ΔP_e is the total electrical power deviation, and its value is expressed in pu.
- ΔP is the total power imbalance, and its value is expressed in pu.

In the present work the mechanical power deviation is neglected and the power imbalance is expressed as:

$$\Delta P = P_{Loss} + P_{Prim} \tag{6}$$

$$P_{Prim} = k \cdot \Delta f_{COI} \qquad \forall \quad t \geq t_{Recovery} \tag{7}$$

Where:

- P_{Prim} is the power of the primary response or the Governors Frequency Response (GFR) of the system that for our study is expressed as a proportional value of the frequency variation Δf_{COI}.
- k is the proportionality constant found from the solution of the power swing equation (k = 1700).
- $t_{Recovery}$ is the total time elapsed ($t_{Recovery}$=5) computed from the initial time (t_{Ini}=1) for the excursion analysis before the disturbance until the time of activation of the primary response ($t_{PrimResp}$=4).

It is known that the P_{Prim} typically starts to be deployed with a time delay of about 2 to 5 seconds after the frequency starts to change and it is fully deployed by about 2 to 4 seconds later. This delay is due to governors dead bands, time constants, and gates or valves velocity limits imposed to avoid equipment damage [23]. Assuming and t_{Ini} = 1 second the P_{Prim} starts at $t_{PrimResp}$ = 4 seconds after the disturbance. With the value of P_{Loss} for our case of study obtained using the methodology of the worst-case contingency analysis, the differential equation can be solved by varying the value of H_{Sys} in Dymola [24](Dynamic Modeling Laboratory) modeling tool, where the calculation intervals were defined to meet the safe operational limits established in the previous paragraph. The plot of the solution is presented in Fig.3. From this computation, the values of the frequency nadir, the recovery time and the primary power response were obtained, and they are presented in Table 1.

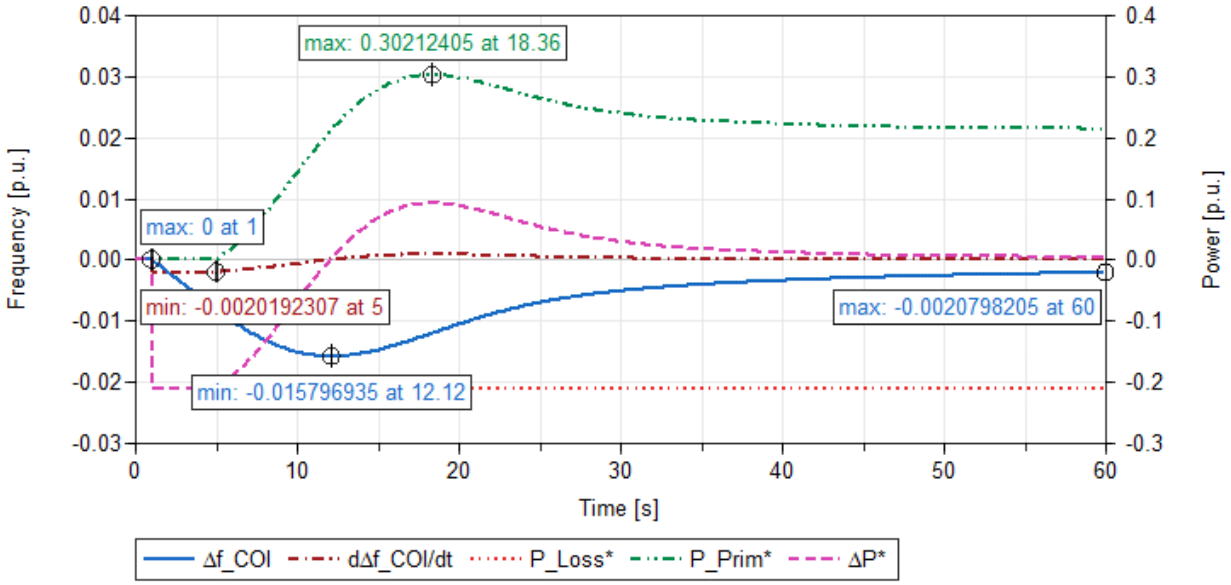

Figure 3: Plot of power swing equation solution, Frequency and Power excursion (worst-case contingency)

2.2.5. RoCoF Estimation

RoCoF is fully determined by the system inertia [25]. RoCoF during a disturbance can be obtained with different measurement approaches that take into account the transient-type changes in frequency. However, to reduce this computation's complexity, the system's damping effect and the noises are neglected. Therefore, the value for the minimum RoCoF can be roughly approximated by measuring the minimum value of $d\Delta f_{COI}/dt$ which is a negative value:

$$RoCoF_{Min} = Min\left(\frac{d\Delta f_{COI}}{dt}\right) \tag{8}$$

Where:

- $RoCoF_{Min}$ is the minimum rate of change of frequency, expressed in pu.

2.2.6. Frequency Nadir Estimation

The frequency nadir can be estimated measuring the lowest point of Δf_{COI} and computing the following equation:

$$f_{Nadir} = \left(1 - Min\left(\Delta f_{COI}\right)\right) \cdot f_{Base} \tag{9}$$

Where:

- f_{Base} is the frequency base, expressed in Hz.(f_{Base} = 50Hz).
- f_{Nadir} is the frequency nadir, expressed in Hz.

2.2.7. Inertia Limit Estimation

The Inertia Limit (H_{Limit}) can be estimated by differentiating the equation (4). By considering all rotating masses on the system aggregated into a single mass, the inertia limit found for our system is H_{Limit} = 52[s]. On this solution, it can be observed from Fig.3 that after a disturbance that causes a loss of generation, the system registers the minimum value of RoCoF (-0.002 p.u./s or -0.1Hz/s) from the moment the disturbance occurs at time=1s until the activation of the system's primary response at time=5s (note that $t_{PrimResp}$ = 4s). Following the system registers the minimum value of frequency (f_{Nadir} = 0.984 p.u. or 49.2Hz) at time=12.12s. And finally, the frequency of the system recovers to be above 49.5Hz. before 60s. All these values meet the safe operational limits.

2.3. Inertia Constraint Implementation

Besides the production/demand balance, and the reserve requirements (upwards and downwards) in each node. The inertia constraint must be met as well. The parameters obtained with the methodology and equations explained previously are presented in Table 1:

Table 1: Determined parameters for inertia limit estimation.

Parameter	Sampled Value	Estimated Value	Assumed Value	Values in p.u.	Equation
$P_{PreDist}(MW)$	1094	-	-	-	(2)
$P_{Loss}(MW)$	190	-	-	-0.21	(4)
$f_{Nadir}(Hz)$	-	49.2	-	0.984	(9)
$Min\Delta f_{COI}(Hz)$	-	0.8	-	-0.01579	(9)
$t_{PrimResp}(s)$	-	-	4	-	(7)
$RoCoF_{Min}(Hz/s)$	-	-0.1	-	-0.002	(8)
$H_{Limit}(s)$	-	52	-	-	(5)

It should be noted that the computation of the limit of inertia in the worst-case contingency scenario was performed offline from the optimization. The implementation of the mathematical equation into the UC/OD model follows this computation. To achieve this, the system inertia is computed by summing up the inertia stored in every committed conventional unit. The system inertia should fulfill the inertia limit at all times, and this new constraint is implemented in the model as:

$$H_{Sys_i} = \sum_u Committed_{u,i} \cdot H_u \quad ; \quad H_{Sys_i} \geq H_{Limit} \tag{10}$$

Where:

- u is the set for all the generation units.
- H_{Sys_i} is the computed inertia of the system at each time-step of simulation.
- $Committed_{u,i}$ is the binary commitment status (1 or 0) for each generation unit at each simulation time-step.
- H_u is the inertia constant of each generation unit. The inertia constants were assumed from typical values found in Table 3.

3. Modelling

3.1. Dispa-SET

The UC/OD energy model used for this study is Dispa-SET. The model solves the optimization of energy systems operation by minimizing the power system's total costs with the use of Mixed-Integer Linear Programming (MILP). This tool has been used in previous works [26] to asses power systems adequacy and flexibility. By being an open-source model, Dispa-SET optimization data can be reused, improved, and reconfigured depending on the desired level of accuracy and complexity. The simulations for this study were conducted using the following approaches:

- The secondary and tertiary reserves were calculated with the probabilistic approach.
- The simulation is formulated as binary formulation. This provides a more accurate representation of the power system operation and allows for the observation of the participation of each unit during the modeling period.

Furthermore, it is important to highlight the flexibility and adaptability of this model to incorporate new features, methodologies, and functionalities to be tested as new simulation options. In this study, two new features were implemented and tested on the Dispa-SET modeling tool. A brief summary comparing the configuration of the model used in the previous work and this work is presented in Table 2:

- The DC-PowerFlow simulation option with the use of an equivalent PTDF matrix.
- The stability and inertia constrain with an off-line estimation of the inertia limit.

The study has been done by activating both features in the model configuration. However, this paper is focused on evaluating the stability and system inertia estimation method and analysing the results related to this feature. For more details on the Dispa-SET modeling framework, please refer to [27].

3.2. Test Case: The Bolivian Power System

The Bolivian Power System (SIN, Sistema Interconectado Nacional) is the test case of the present study. The SIN has previously been examined in [26]. An updated one-line scheme is presented in Fig.4. To enhance

Table 2: Differences between Simulation Configurations (Previous - Present).

Dispa-SET Simulation Options		Previous Study	Present Study
Horizon	Simulation	2020	2026
Simulation Options	Simulation type	Clustering	No clustering
	Reserve calculation	Generic	Probabilistic
	Transmission grid type	NTC	DC-Power Flow
	Inertia Constraint	False	True

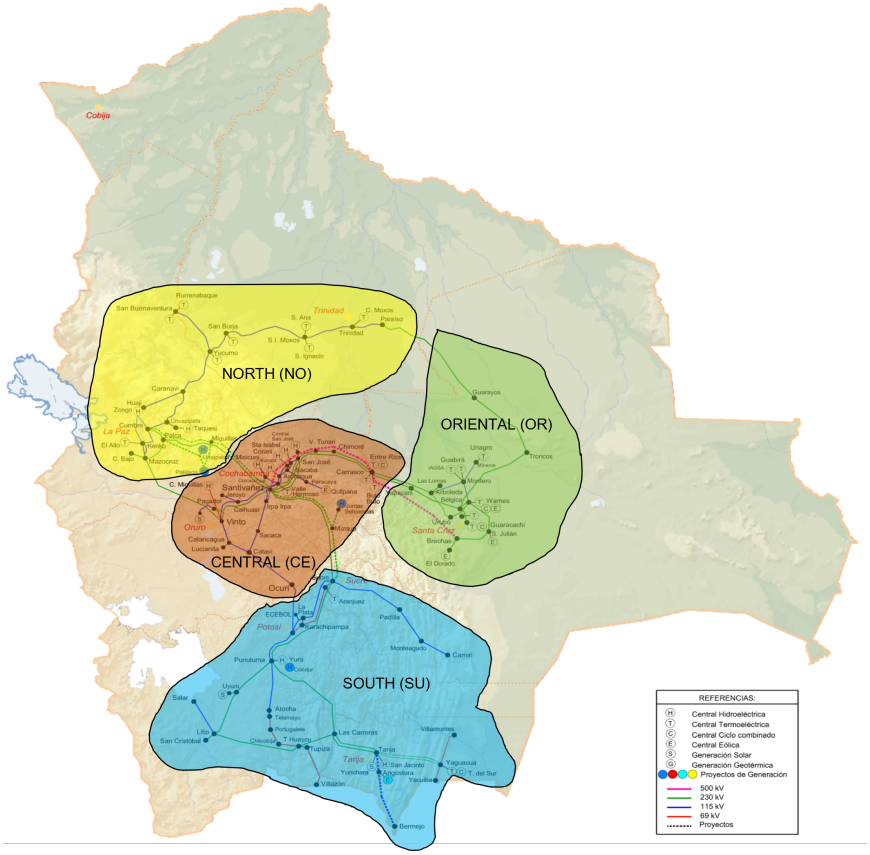

Figure 4: The SIN layout implemented and planned in the period 2026. [28]

the accuracy of the analysis, a comprehensive review of the relevant database provided by the owner of the Bolivian grid (ENDE), was undertook. The database for the year 2026 was obtained from the Stochastic dual dynamic programming (SDDP) model. The necessary adaptations were made to update the database used in [26] with the use of ENDE database. Since the main scope of this work is mainly to introduce a stability and reserve constraint in our UC/OD model, the detailed description of the input data origin is irrelevant. However, for further comprehension of it, please refer to [29].

Moreover, it is important to note that the input-data used in our model was specifically designed for constructing a test case for the implemented features and the methodology rather than representing the true operational values of the power system under examination. Therefore, it is essential to consider the following factors when interpreting our results:

- As in [26], the power plant data has been roughly assumed from typical values for each type of generator.
- This Is the first time introducing the inertia constant (H) as a parameter into the Dispa-SET model. The values of this constant were assumed from typical values according to each generator's characteristics, the reference values were taken from the Table 3.

3.3. Scenarios

The impact of introducing an inertia constraint while increasing the installed power capacity of VRE on the performance of the power system was investigated in this study. The baseline scenario (S0, M0) represents

Table 3: Summary of inertia values (H) for different generation types

Type of generating unit	Rated Power	H (s)	Reference	Year
Thermal	10 - 1500 MW	2 - 8	[30]	2012
Thermal (combined cycle)	115 MW	4.3	[31]	2012
Thermal (gas)	90 - 120 MW	5	[31]	2012
Hydroelectric 80 $<$n $<$514 rpm	10 - 65 MW	1.75 - 4.3	[30]	2008
Hydroelectric	Not indicated	2 - 4.75	[32]	2013

the planned conditions for the system by the year 2026, while multiple scenarios were formulated by scaling up the installed power capacity of VRE (solar and wind energy in this case). In each scenario, the installed power capacities of other technologies were kept unchanged, and the current locations of VRE units were conserved.

A batch of UC/OD simulations were optimized in the model, including each scenario without the inertia constraint (S0-S5) and with the inertia constraint (M0-M5). The results were evaluated by performing a sensitivity analysis comparing the simulations with and without the new inertia constraint. Table 4 summarizes the variations in the simulation environment for each penetration scenario.

Table 4: Installed power capacity by technology and per scenario

Scenario/Technology		GTUR Gas	GTUR Diesel	COMC Gas	BIO Bio	HDAM Wat	WTON Win	PHOT Sun	Total
S0,M0	Inst. Cap.(MW)	636.48	11.74	2053.81	77.23	1218.77	173.58	162.85	4334.46
S1,M1	Inst. Cap.(MW)	636.48	11.74	2053.81	77.23	1218.77	694.32	651.4	5343.75
S2,M2	Inst. Cap.(MW)	636.48	11.74	2053.81	77.23	1218.77	1041.48	977.10	6016.61
S3,M3	Inst. Cap.(MW)	636.48	11.74	2053.81	77.23	1218.77	1562.22	1465.65	7025.90
S4,M4	Inst. Cap.(MW)	636.48	11.74	2053.81	77.23	1218.77	2082.96	1954.20	8035.19
S5,M5	Inst. Cap.(MW)	636.48	11.74	2053.81	77.23	1218.77	2603.70	2442.75	9044.48

4. Results and Discussion

4.1. Sensitivity Analysis: Impacts of Inertia Constraint on results

The scenarios studied provide valuable insights into the potential impact of increasing VRE penetration on the power system, emphasizing the significance of considering the system's constraints and limitations in future planning and development. Table 5 summarizes the values for which their sensitivity to the new inertia constraint is assessed.

Table 5: Results Summary

Scenario	Inertia Limit sec.	Inertia Ave. sec.	Inertia Min sec.	Inertia Max sec.	Total Curt. TWh	Total ShedLoad MWh	Shadow Price Ave. eur/kWh	VRE Gen. TWh	Total Gen. TWh	VRE Penetration%
S0	-	127.63	59.31	165.25	0.02	551.17	10.32	0.88	11.44	7.65
M0	52	127.21	59.55	165.25	0.02	291.31	10.90	0.88	11.44	7.65
S1	-	106.45	47.7.83	146.25	0.43	481.69	9.31	3.16	11.44	27.57
M1	52	107.06	54.52	152.25	0.43	511.06	10.11	3.15	11.44	27.56
S2	-	95.29	42.35	136.25	0.91	415.15	7.93	4.47	11.44	39.10
M2	52	96.43	52.1	141.25	0.93	397.08	8.39	4.49	11.44	39.04
S3	-	66.80	14.8	122.25	2.24	233.25	3.87	5.84	11.44	51.04
M3	52	74.41	52.00	122.25	2.27	130.26	3.99	5.81	11.44	50.76
S4	-	56.49	11.50	117.25	4.55	121.21	2.06	6.23	11.44	54.42
M4	52	69.09	52.05	117.25	4.66	233.94	2.48	6.14	11.44	53.66
S5	-	50.31	12	94.55	6.99	10.09	0.56	6.49	11.44	56.68
M5	52	65.08	52	107.25	7.13	161.76	1.12	6.38	11.44	55.81

System Inertia

Figure 5 presents the analysis of the model's response to the newly introduced inertia constraint. It shows a comparison of the system's inertia time series, both with and without the inclusion of this constraint, denoted as (M1-M5) and (S1-S5), respectively. It is notable that the inertia's lower limit is automatically raised to the value imposed in the model. Additionally, Figure 6 shows that for scenarios with low/mid (S0-S2) penetration levels of VRE, the system's inertia is distributed on a broader frame and reaches very high levels exceeding 80 seconds from 20% to 75% of the year. The system barely operates under the inertia limit, set at 52 seconds. This suggests large system robustness, which implies proper conditions for implementing new energy policies and technologies to force VRE penetration and reduce curtailment. On the other hand, for the scenarios with higher penetration levels of VRE (S3-S5), the system's inertia frame is narrower, and the system operates under the inertia limit, set at 52 seconds, approximately from 15% to 55% of the year, which can lead to risky operation in the event of N-1 contingencies. However, the levels, periods, and locations with a higher probability of under-frequency protection tripping should be studied individually.

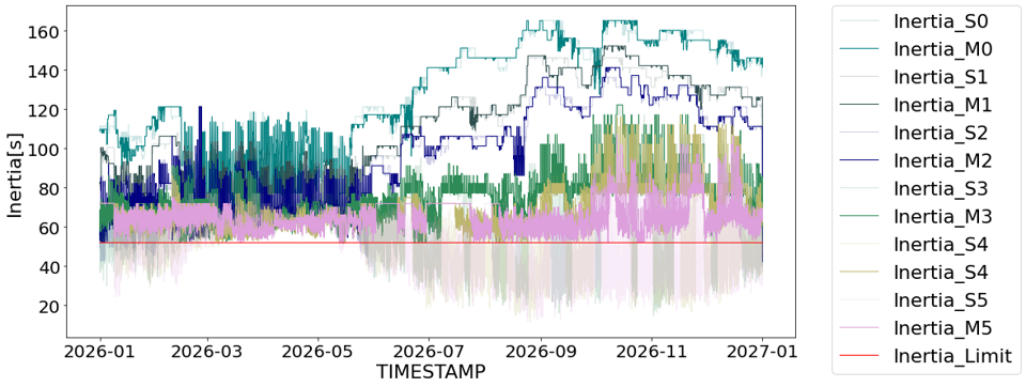

Figure 5: System Inertia time series S5 and M5 (period: Sep 1st-7th of 2026)

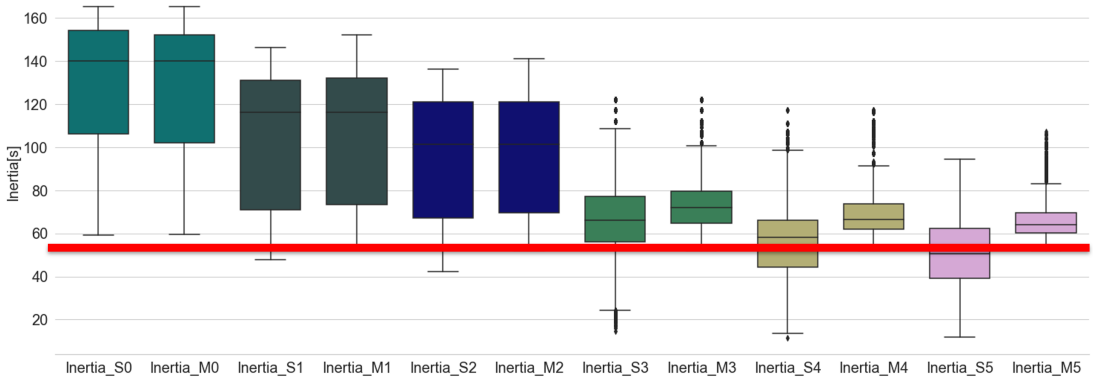

Figure 6: Cumulative Distribution for system inertia for different scenarios of VRE penetration

VRE Penetration

After conducting a comparative analysis between simulated scenarios with and without the implementation of inertia limits, it can be deduced that the newly imposed restriction does not seem to impede the integration of renewable energy sources. This suggests that the electrical system being studied is quite robust, likely due to the presence of significant hydropower capacity installed. Moreover, it might be assumed that the installed capacity of VRE is directly proportional to the penetration and usage of this technology. However, as shown in Table 5, even as the installed capacity of VRE increases in subsequent scenarios from (S3) and (M3), the penetration of VRE tends to remain close to 50%. Thus, it appears that other factors, such as the installed hydropower capacity, may play a role in limiting further penetration of VRE beyond this point. That can be confirmed by observing the VRE Penetration Level time series across the year Figure 7; this figure shows that the highest penetration of VRE takes place during the dry season (from June to December).

Curtailment

Similar to VRE penetration, the new inertia constraint does not significantly affect curtailment. However, as can be noted from Figure 8, as VRE capacity increases beyond scenario 3, curtailment also increases, displaying

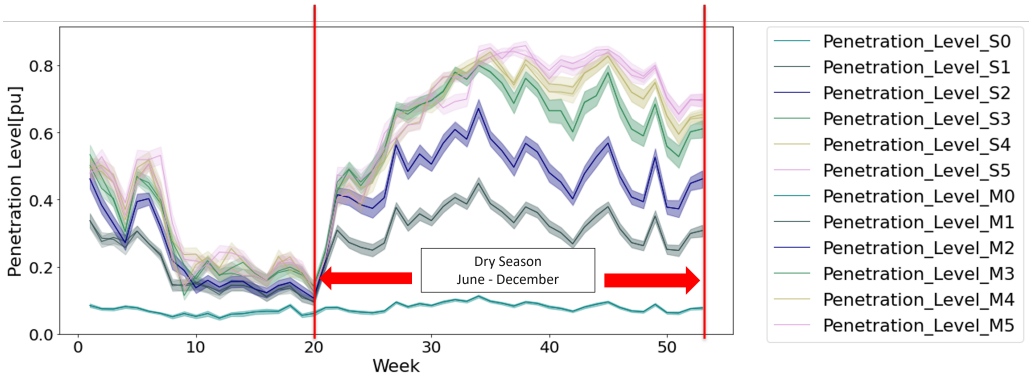

Figure 7: Penetration level of VRE for each month of the period 2026.

an exponential curve with a limit on VRE penetration. It can also be noted that the highest amount of curtailment occurs during the wet season, further reinforcing the argument that the installed hydropower capacity plays a significant role in limiting the penetration of VRE.

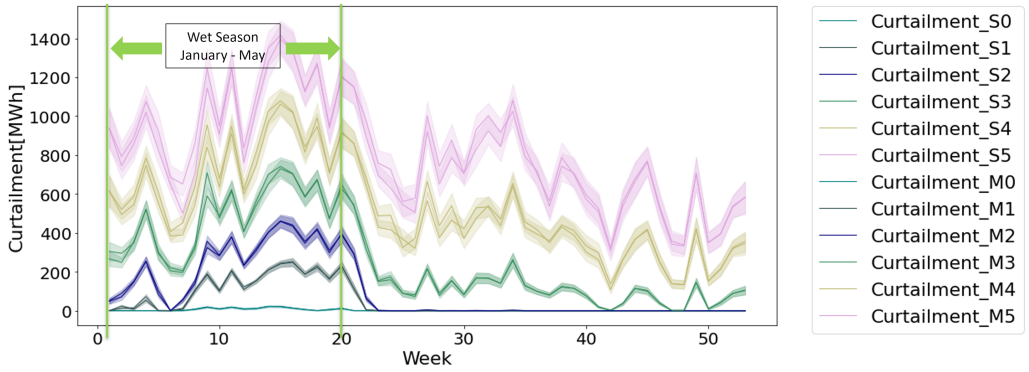

Figure 8: Curtailment of VRE for each month of the period 2026.

Load Shedding

In all scenarios, the largest load shedding is approximately 1 MWh, which is negligible. This indicates that the system can effectively meet the demand throughout the year and highlights the efficient functioning of interconnections through transmission lines. Additionally, the new inertia limit does not impact the load-shedding values.

Shadow Price

Table 5 shows that the new inertia constraint does not impact the first three scenarios, where VRE generation is committed to replacing thermal generation. However, in scenarios S4 and S5, VRE generation is committed to replacing hydro units, increasing energy costs. Moreover, in scenarios M4 and M5, the inertia limits force the commitment of hydro units, leading to higher prices. However, it can be noted that the impact of inertia on the energy price is not high compared to the necessary investment to install very high levels of VRE.

5. Conclusions

The present work proposes an efficient methodology to estimate a power system's inertia limit under a worst-case contingency scenario N-1. By introducing this limit as a constraint in the UC/OD model, a safer operation can be ensured even under scenarios with high penetrations of VRE. The constraint was established through a deterministic approach sampling the minimum conventional power committed and then considering the worst-case contingency on this sampled period, with the purpose of computing the post-fault variables by solving the power swing equation and finally obtaining the value of the inertia limit. With the new inertia constraint set, simulations were conducted to evaluate its impact on curtailment, load shedding, VRE penetration level, and energy generation cost, applying a sensitivity analysis.

The results show that inertia constraint only becomes significant under high penetration of VRE. This can be attributed to the significant amounts of hydropower committed in the dispatch. On one side, it is positive because it ensures robustness, particularly during the wet season; on the other side, a dispatch predominantly reliant on hydropower can result in the vulnerability of the system to hydrological variations due to climate

changes. This raises concerns about the adequacy of storage and battery systems and the shallow penetration levels of VRE, specifically during the wet season.

In the specific case of this study, since VRE availability is considerable throughout the year, there is potential to enhance the complementarity between VRE and hydropower. This can be achieved by investing in additional hydro dams to store energy for the dry season. Such infrastructure could help maintain more consistent inertia throughout the year, addressing the simulations' limitations.

Periods have been identified where the system inertia is lower than the safe limit of inertia. These periods of risk account from 15% to 55% of the year, depending on the scenario, if the limit of inertia is not imposed as a constraint in the UC/OD model.

Overall, implementing the inertia constraint allows for the assessment of periods of risk quantitatively and guarantees safer power system operation, even under challenging conditions. The results of this work provide important insights for future studies, such as considering the implementation of an upper inertia limit to force higher VRE penetration and a more balanced mix in the commitment. Additionally, using inertia limits as a grid code could lead to determining a potential methodology for battery sizing and studying the system complementarity of the energy mix. However, it is essential to note that the deterministic approach may not fully capture the stochastic behavior of the system, and the simplifications made in the model should be carefully considered when interpreting the results.

Finally, we can conclude that the size of inertia is not the sole factor to consider, but its allocation is also crucial, requiring further exploration in future studies. The methodology can be improved by incorporating regional or zonal calculations for the inertia constraint. Additionally, analyzing the complementarity between hydropower and VRE under various rainfall and water storage scenarios would provide valuable insights into hydropower's contribution to the overall robustness of power systems. These avenues of research hold the potential for a deeper understanding of system dynamics and optimization.

Acknowledgments

The authors gratefully acknowledge the financial support and resources provided by the ARES-CDD and ARES PRDBOL2022 programmes, which were instrumental in the successful completion of this work.

References

[1] SDG Indicators — SDG Indicators.

[2] World Energy Outlook 2022 – Analysis.

[3] B. Kroposki, B. Johnson, Y. Zhang, V. Gevorgian, P. Denholm, B. Hodge, and B. Hannegan. Achieving a 100% Renewable Grid: Operating Electric Power Systems with Extremely High Levels of Variable Renewable Energy. *IEEE Power and Energy Magazine*, 15(2):61–73, March 2017.

[4] Q. Hou, E. Du, N. Zhang, and C. Kang. Impact of High Renewable Penetration on the Power System Operation Mode: A Data-Driven Approach. *IEEE Transactions on Power Systems*, 35(1):731–741, January 2020.

[5] Andreas Ulbig, Theodor S. Borsche, and Göran Andersson. Impact of Low Rotational Inertia on Power System Stability and Operation. *IFAC Proceedings Volumes*, 47(3):7290–7297, January 2014.

[6] E Ela, M Milligan, and B Kirby. Operating Reserves and Variable Generation. Technical Report NREL/TP-5500-51978, 1023095, August 2011.

[7] NATHAN COHN. *Control of Generation and Power Flow on Interconnected Systems*. JOHN WILEY AND SONS, INC., January 1961.

[8] Operational limits and conditions for mutual frequency support over hvdc.

[9] Filippo Bovera, Giuliano Rancilio, Davide Falabretti, and Marco Merlo. Data-Driven Evaluation of Secondary- and Tertiary-Reserve Needs with High Renewables Penetration: The Italian Case. *Energies*, 14(8):2157, January 2021. Number: 8 Publisher: Multidisciplinary Digital Publishing Institute.

[10] Review of the System Black Event in South Australia on 28 September 2016.

[11] GB power system disruption on 9 August 2019: Final report. *Final report*.

[12] B. Tan, J. Zhao, M. Netto, V. Krishnan, V. Terzija, and Y. Zhang. Power System Inertia Estimation: Review of Methods and the Impacts of Converter-Interfaced Generations. *International Journal of Electrical Power & Energy Systems*, 134, July 2021.

[13] Ervin Spahic, Deepak Varma, Günther Beck, German Kuhn, and Volker Hild. Impact of reduced system inertia on stable power system operation and an overview of possible solutions. In *2016 IEEE Power and Energy Society General Meeting (PESGM)*, pages 1–5, July 2016. ISSN: 1944-9933.

[14] M. McPherson and S. Tahseen. Deploying storage assets to facilitate variable renewable energy integration: The impacts of grid flexibility, renewable penetration, and market structure. *Energy*, 145:856–870, February 2018.

[15] David S. Renné. Emerging Meteorological Requirements to Support High Penetrations of Variable Renewable Energy Sources: Solar Energy. In Alberto Troccoli, Laurent Dubus, and Sue Ellen Haupt, editors, *Weather Matters for Energy*, pages 257–273. Springer, New York, NY, 2014.

[16] Peng Wang, Ershun Du, Ning Zhang, Xinzhi Xu, and Yi Gao. Power system planning with high renewable energy penetration considering demand response. *Global Energy Interconnection*, 4(1):69–80, February 2021.

[17] L. Mehigan, Dlzar Al Kez, Seán Collins, Aoife Foley, Brian Ó'Gallachóir, and Paul Deane. Renewables in the European power system and the impact on system rotational inertia. *Energy*, 203:117776, July 2020.

[18] Khalid Mehmood Cheema. A comprehensive review of virtual synchronous generator. *International Journal of Electrical Power & Energy Systems*, 120:106006, September 2020.

[19] L. Meng, J. Zafar, S. K. Khadem, A. Collinson, K. C. Murchie, Federico C., and Graeme M. B. Fast Frequency Response From Energy Storage Systems—A Review of Grid Standards, Projects and Technical Issues. *IEEE Transactions on Smart Grid*, 11(2):1566–1581, March 2020.

[20] Y. Zhang, H. Cui, J. Liu, F. Qiu, T. Hong, R. Yao, and F. Li. Encoding Frequency Constraints in Preventive Unit Commitment Using Deep Learning With Region-of-Interest Active Sampling. *IEEE Transactions on Power Systems*, 37(3):1942–1955, May 2022. Conference Name: IEEE Transactions on Power Systems.

[21] Ziyang Zhang, Ershun Du, Fei Teng, Ning Zhang, and Chongqing Kang. Modeling Frequency Dynamics in Unit Commitment With a High Share of Renewable Energy. *IEEE Transactions on Power Systems*, 35(6):4383–4395, November 2020. Conference Name: IEEE Transactions on Power Systems.

[22] Luis Badesa, Fei Teng, and Goran Strbac. Conditions for Regional Frequency Stability in Power System Scheduling – Part II: Application to Unit Commitment. *IEEE Transactions on Power Systems*, 36(6):5567–5577, November 2021. arXiv:2009.13164 [cs, eess, math].

[23] Berardino Porretta and Steven Porretta. Calculation of power systems inertia and frequency response. In *2018 IEEE Texas Power and Energy Conference (TPEC)*, pages 1–6, February 2018.

[24] Dymola - Dassault Systèmes®.

[25] Graeme Chown, Jarrad Wright, Robbie van Heerden, and Mike Coker. System inertia and Rate of Change of Frequency (RoCoF) with increasing non-synchronous renewable energy penetration. *CIGRE Science and Engineering*, 11, June 2018.

[26] M. Navia, R. Orellana, S. Zaráte, M. Villazón, S. Balderrama, and S. Quoilin. Energy Transition Planning with High Penetration of Variable Renewable Energy in Developing Countries: The Case of the Bolivian Interconnected Power System. *Energies*, 15(3):968, January 2022. Number: 3 Publisher: MDPI.

[27] The Dispa-SET model — Documentation.

[28] Comité Nacional de Despacho de Carga. Programación de mediano plazo en el sistema interconectado nacional, 2022.

[29] Huallpara A., Navia M., Gomand I., Balderrama S., Pavicevic M., and Quoilin S. Comparative analysis of dynamic and linear programming energy systems models applied to the bolivian power system. page 12, June 2023. Publisher: ECOS 2023 - The 36TH International Conference on Efficiency, Cost, Optimization, Simulation and Environmental Impact of Energy Systems.

[30] Paul M. Anderson and A. A. Fouad. *Power System Control and Stability*. John Wiley & Sons, 2 edition, 2002.

[31] P. Tielens and D. Hertem. Grid Inertia and Frequency Control in Power Systems with High Penetration of Renewables. 2012.

[32] M. Shahidehpour, M. Eremia, and L. Toma. Modeling the Main Components of the Classical Power Plants. In *Handbook of Electrical Power System Dynamics*, volume 92 of *IEEE Press Series on Power Engineering*, pages 137–178. Wiley, Hoboken, NJ, USA, 1 edition, 2013.